# (x)ZnO(1 − x)$Fe_2O_3$ nanocrystallines for the removal of cadmium(II) and nickel(II) from water: kinetic and adsorption studies

L. Khezami, Kamal K. Taha, Mohamed OuldM'hamed and O. M. Lemine

## ABSTRACT

In this work the efficiency of mechanically prepared magnetic (x)ZnO(1 − x)$Fe_2O_3$ nanocrystallines for Ni(II) and Cd(II) ions removal was investigated. The produced nanoparticles were characterized using $N_2$ adsorption, X-ray diffraction (XRD), and magnetization techniques. Batch mode experiments were performed to evaluate the parameters of the heavy metal ions adsorption on the nanoparticles. The concentration and temperature were found to be detrimental factors in the adsorption process as the amounts adsorbed were enhanced by their increase. While Cd(II) adsorption was found to comply with the Langmuir isotherm, the adsorption of Ni(II) ions fitted both Langmuir and Freundlich isotherms. The pseudo-second-order model was the kinetics model describing the adsorption process. The adsorption process was endothermic and spontaneous as indicated by the thermodynamic study results. The positive entropy obtained may suggest increased randomness at the solid–solution interface. A mechanism for the metal ions adsorption was proposed.

**Key words** | magnetic properties, metal ions removal, XRD, (x)ZnO(1 − x)$Fe_2O_3$

**L. Khezami**
**Kamal K. Taha** (corresponding author)
**Mohamed OuldM'hamed**
Department of Chemistry, College of Science,
Al Imam Mohammad Ibn Saud Islamic University (IMSIU),
Riyadh 11432,
Saudi Arabia
E-mail: *kamaltha60@gmail.com*

**O. M. Lemine**
Department of Physics, College of Science,
Al Imam Mohammad Ibn Saud Islamic University (IMSIU),
Riyadh,
Saudi Arabia

**Kamal K. Taha**
Department of Chemistry & Industrial Chemistry,
College of Applied & Industrial Sciences, University of Bahri,
Khartoum,
Sudan

## INTRODUCTION

Due to the great boom of the world population, the demand for clean healthy water is progressively increasing. Still, considerable amounts of lethal chemicals, such as dyes, pharmaceuticals, and metal ions are discharged into water systems. As a consequence of human, urban, and industrial activities, the problem is aggravated. Heavy metal ions usually enter into human bodies through food chains. Their accumulation may lead to serious diseases and/or damage, if ingested beyond their tolerance limits. Such harmful effects can extend to the environment also. To minimize their hazardous impact on both biota and environment, metal ions contaminated water treatment is of high priority (Babel & Kurniawan 2004).

The toxic heavy metal, cadmium, is discharged to ecosystems through processes such as fuel combustion, metal production, fertilizers' application, metal finishing, and industry. Thus, the level of cadmium reaches a μg $L^{-1}$ to mg $L^{-1}$ range exceeding its 10 and 100 ng $L^{-1}$ level in natural water as a result of such anthropogenic activities (Nordberg *et al.* 2014). Cadmium is a carcinogenic and teratogenic agent that affect adult and fetus internal organs (Boparai *et al.* 2011).

Similarly, nickel is a toxic metal found in the environment, which can cause respiratory tract carcinogenesis and allergic contact dermatitis once it enters the human body. Industries such as stainless steel and nickel electroplating are sources of Ni(II) in the environment (Meena *et al.* 2005).

Heavy metal ions are removed from water and wastewater by means of membrane filtration, liquid extraction, electro-dialysis, chemical precipitation, ion exchange (Fu & Wang 2011), along with other methods. For small-scale industries and domestic uses, these methods are not appropriate as they are costly with low feasibility (Li *et al.* 2007).

doi: 10.2166/aqua.2017.033

On the other hand, adsorption is a more feasible technique that can be employed in industrial application using natural or synthetic materials. Thus, clays, zeolites, biomass, activated carbon, dried plant parts, saw dust, and biopolymers are used due to their abundance and low cost (Singh *et al.* 1998; Li *et al.* 2010).

Nowadays, nanomaterials are gaining significant importance in adsorption processes due to their great ability to remove pollutants from aqueous media. Their capacity to adsorb pollutants is due to the large surface to volume ratio along with the ease of tailoring of their surface properties by modifying their functionality and morphology (Roy *et al.* 2005; Ramana *et al.* 2013; Roy & Bhattacharya 2013; Arce *et al.* 2015).

Magnetic nanomaterials are becoming a focus of new research due to their being environmentally pleasant, naturally available, and easily recoverable. Due to its magnetic properties, iron oxide is extensively employed in water treatment for the efficient removal of contaminants (Tang & Lo 2013). Moreover, iron oxide nanoparticles can be functionalized to improve their adsorption and photocatalytic activity (Xu *et al.* 2012). Metal ferrites ($MFe_2O_4$) were obtained by incorporating oxides of cobalt (Ding *et al.* 2015; Nassar & Khatab 2016), manganese (Bhowmik *et al.* 2016), or calcium (Debnath *et al.* 2016) into iron oxide and were applied in the removal of dyes or heavy metal ions. Being non-toxic, environmentally harmless, cheap, and structurally stable, ($ZnFe_2O_4$) is a promising candidate for many applications (Reddy & Yun 2016). The co-presence of ferric and ferrous ion in its spinel structure provides it with wonderful properties that make it a focus of extensive research in different fields and applications (Kale *et al.* 2004; Thirupathi & Singh 2015).

In this work, (x)ZnO(1 – x)$Fe_2O_3$ has been fabricated and characterized. The effects of some experimental parameters such as initial concentration and temperature and on Cd(II) and Ni(II) removal were studied. Mathematical models were applied to describe the adsorption process and obtain the different parameters. Adsorption isotherms were modeled using the Langmuir and Freundlich equations. The kinetics of the process was investigated under the first- and second-order rate laws. Parameters such as rate constants, adsorption capacities, thermodynamic function variations ($\Delta H^o$, $\Delta S^o$, and $\Delta G^o$) were determined and their effect on the adsorption was scrutinized.

## METHODOLOGY

### Materials

Equimolar amounts of hematite ($\alpha$-$Fe_2O_3$) and zinc oxide (ZnO) were mixed in a planetary milling (Fritsch-P7) and milled for 10 hours at 700 rpm and 10:1 ball to sample mass ratio. The crystallite structure of the nano-particles was investigated by X-ray powder diffraction (XRD) analysis using a diffractometer (D8) equipped with Cu-K$\alpha$ radiation ($\lambda = 1.5418$ Å). The specific area and pore size were characterized by $N_2$ adsorption–desorption carried out at 77 K in ASAP 2020 (Micromeritics) equipment. Prior to conducting the adsorption experiment, the sample was degassed with helium at 250 °C for 2.0 h to remove humidity and adsorbed impurities. The BET (Brunauer, Emmett, and Teller) equation and t-plot method of Lippens & De Boer (1965) were employed in the pores' surface area calculations.

Nickel nitrate ($Ni(NO_3)_2$) and cadmium nitrate ($Cd(NO_3)_2$ salts were used to prepare aqueous (1,000 mg $L^{-1}$) stock solution of Ni(II) and Cd(II), respectively. Desired concentrations were obtained by appropriate dilutions. NaOH and $HNO_3$ solutions were used to adjust the pH. All the reagents were from Sigma-Aldrich and were used as received.

Experiments were performed in batch mode by mixing $10 \pm 0.1$ mg of ($ZnFe_2O_4$), to 25 mL of a known Ni(II) and Cd(II) solution concentration in a 50 mL Erlenmeyer flask. Adsorption studies were conducted at pH 7.0 and initial Ni(II) and Cd(II) concentrations in the range of 25–125 mg·$L^{-1}$ to obtain equilibrium isotherms. A number of flasks were placed on a multi-position magnetic stirrer and stirred individually at 600 rpm. About a 15 mL portion of the solution was taken after 12 h contact time, centrifuged (centrifuge, Hettich Zentrifugen EBA 20), and then filtered. Residual nickel and cadmium ions content of filtrate were determined by atomic emission spectroscopy equipment (Genius, ICP-EOS, Germany).

### Methods

The size of the crystalline magnetic particles was obtained from the XRD data using the Scherer equation:

$$D = \frac{k\lambda}{B\cos\theta} \quad (1)$$

where $B$ is the full width at half maximum (*FWHM*) of the peak (in radians), the constant $k$ has a value of ≈0.89, $\theta$ is diffraction angle, and $\lambda$ for Cu-K$\alpha$ is 1.5418 Å. The magnetic properties of the prepared nanopowder were measured at ambient temperature via a Lake Shore 4700 model magnetometer (VSM) with a magnet of 2 Tesla strength.

According to Equation (2), the mass ($mg$) of Ni(II) or Cd(II) removed by 1 g of adsorbent $q_e$ is:

$$q_e = \frac{(C_0 - C_e)*\mathrm{V}}{m} \tag{2}$$

At equilibrium, the adsorption is usually described by adsorption isotherms. The Langmuir and Freundlich equations are mostly adopted:

$$\frac{C_e}{q_e} = \frac{1}{q_m} C_e + \frac{1}{q_m.K_L} \text{ linear form of Langmuir equation} \tag{3}$$

$$log q_e = \frac{1}{n} log C_e + log K_F \text{ linear form of Freundlich equation} \tag{4}$$

where $q_e$ (mg·g$^{-1}$) is the mass of solute adsorbed by a unit mass of nanopowder, $C_e$ is the solute concentration at equilibrium (mg·L$^{-1}$), $q_m$ is the mass of Ni(II) and Cd(II) sufficient to cover the site of adsorption forming a monolayer (Weng & Huang 2004), and the constant $K_L$ is indicative of the adsorption free energy value. The slope and intercepts of the $C_e/q_e$ versus $C_e$ graph (Equation (3)) can provide the $q_m$ and $K_L$ values, respectively. We can obtain the values of $k$ and $n$ from the intercept and slope of lo$q_e$ versus log $C_e$ graph (Equation (4)) (Gupta *et al.* 1998).

The prediction of the adsorption kinetics data is tested by either the pseudo-first- or second-order models. The pseudo-first-order kinetics is given by the following equation (Gupta *et al.* 1998):

$$ln(q_e - q_t) = ln(q_e) - k_1.t \tag{5}$$

where $q_t$ (in $mg{\cdot}g^{-1}$) is the mass of metal ions adsorbed by a gram of adsorbent at time $t$ (minutes), and $k_1$ is the constant for adsorption rate in reciprocal minutes. By plotting a graph of ln($q_e$ – $q_t$) against $t$, $q_e$ and $k_1$ can be respectively obtained from the intercept and slope. Sorption kinetics can be also represented by a pseudo-second-order rate law (Ho & McKay 1998):

$$\frac{t}{q_t} = \frac{1}{k_2.q_e^2} + \frac{t}{q_e} \tag{6}$$

Here, $k_2$ represents the constant for adsorption rate (g.mg$^{-1}$·min$^{-1}$). Data satisfying this law will be linear if $t/q_t$ is plotted against $t$. The slope of such a graph gives $q_e$, while $k_2$ value is calculated from the intercept once $q_e$ is known.

The thermodynamic functions ($\Delta H^o$, $\Delta G^o$, and $\Delta S^o$) for the metal ions by zinc ferrite are calculated using the following formulae:

$$\Delta G^o = -R.T.ln(\underset{a}{K}) \tag{7}$$

$$\Delta S^o = \frac{\Delta H^o - \Delta G^o}{T} \tag{8}$$

Equation $K_a = q_m{\cdot}K_L$ can be employed to calculate the equilibrium constant. The $\Delta H^o$ value can be obtained from the $ln(K_a)$) against ($T^{-1}$) plot.

## RESULTS AND DISCUSSION

### Structural and magnetic characterization

#### XRD analysis

Figure 1 shows the diffraction patterns for (x)ZnO(1 – x)$Fe_2O_3$ mixture after 10 hours of milling. It can be seen that the XRD peaks are wider with relatively reduced intensity. Thus, mechanical milling brings about deformations leading to the creation of strained crystals of reduced size. All zinc oxides (ZnO), hematite ($\alpha$-$Fe_2O_3$), and zinc ferrite $ZnFe_2O_4$ phases coexist in the XRD spectrum (Figure 1). This may be attributed to the high ratio of both ZnO and ($\alpha$-$Fe_2O_3$) used to prepare the (x)ZnO(1 – x)$Fe_2O_3$ nanoparticles or to the lesser milling interval as obtaining only $ZnFe_2O_4$ requires a longer time (Chen *et al.* 2013). The

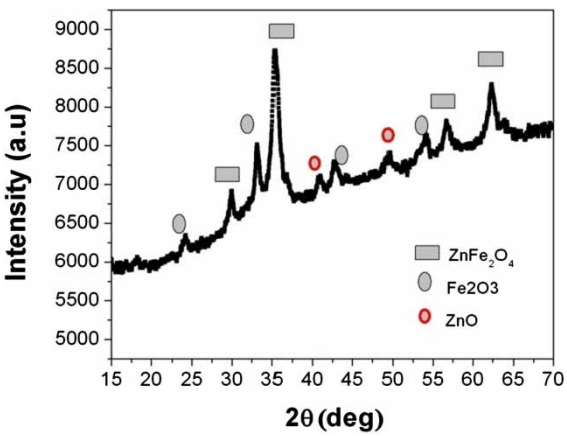


**Figure 1** | X-ray diffraction patterns of ball-milled (x)ZnO(1 – x)$Fe_2O_3$ nanoparticles.

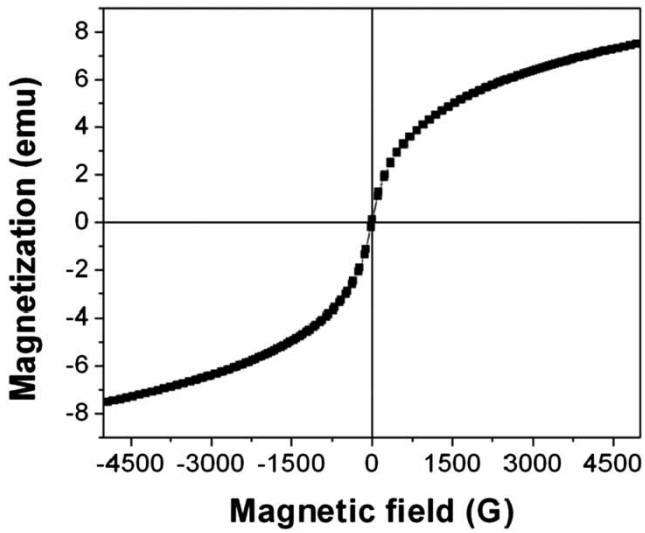


**Figure 2** | Room temperature magnetic hysteresis loop of the ball-milled (x)ZnO(1 – x)$Fe_2O_3$.

coexistence of several phases in this sample usually enhances the adsorption efficiency of the obtained nanocrystallines. Guo *et al.* (2011) reported enhanced photocatalytic activity of $BiFeO_3$ nanoparticles with parasitic $\gamma$-$Fe_2O_3$. This behavior was attributed to the formation of a heterojunction structure between the BFO and $\gamma$-$Fe_2O_3$ phases. The average size of the magnetic crystallite was found to be 110 nm by applying the Scherer formula to the most prominent peak (311).

## Magnetic properties

Magnetic measurement performed at room temperature is shown in Figure 2. It can be observed that the sample is ferromagnetic with 7.5092 emu saturation ($M_S$) and 9 Gauss coercivity field ($H_c$). The ferromagnetic behavior of the mixture due to the presence of $Fe_2O_3$ and zinc ferrite will improve its capacity to adsorb metal ions and pollutants. In an external magnetic field, a correlation between the size or number of atoms of a magnetic particle has been reported. Consequently, higher Ms values of large size particles are due to surface spin effects (Kodama *et al.* 1996). The higher Ms values for the samples under study compared to other data can be correlated to the larger particle size (110 nm) (Mozaffari *et al.* 2010).

## BET surface area analysis

Figure 3 depicts the adsorption–desorption isotherm of adsorbent at the boiling point of $N_2$. It can be clearly seen

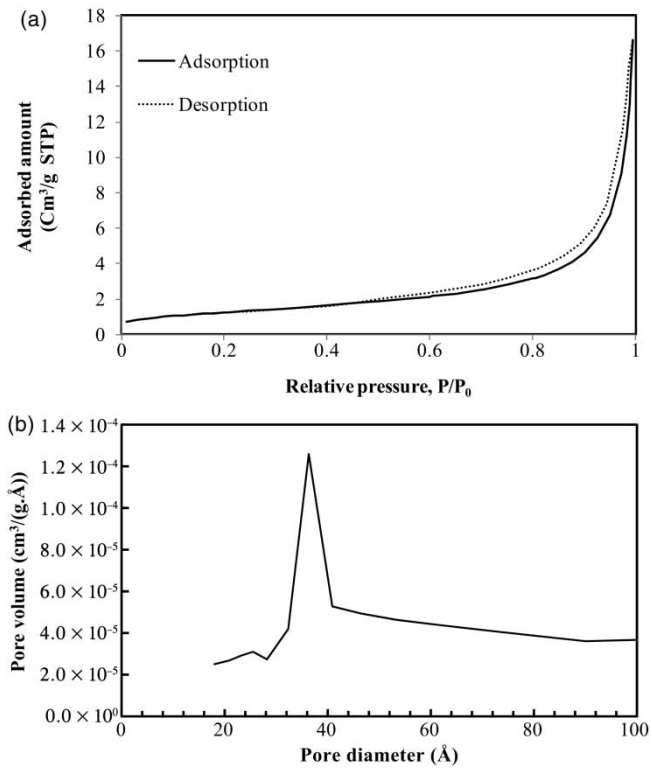


**Figure 3** | (a) $N_2$ adsorption–desorption curves of at 77 K for (x)ZnO(1 – x)$Fe_2O_3$ nanopowder. (b) Pore size distribution for (x)ZnO(1 – x)$Fe_2O_3$ nanopowder.

that the isotherm is of type II, as categorized by the IUPAC and Brunauer (Rouquerol *et al.* 2013). The isotherm is type H4 hysteresis loop, characteristic of aggregated

particles with nonporous or macroporous adsorbents and unrestricted monolayer–multilayer adsorption (Rouquerol *et al.* 2013). The BET analysis revealed particles with $S_{BET}$ 4.51 $m^2 \cdot g^{-1}$ and pores with average volume of 0.0201 $cm^3/g$. Similar values of specific surface area for $ZnFe_2O_4$ were obtained by Sakthivel *et al.* (2002). The relatively small specific area may be attributed to the large particle size (Zhang *et al.* 2010). The data obtained from the analysis are summarized in Table 1.

## Heavy metal ions adsorption study

### Equilibrium study

The heavy metal ions were removed from the solutions at room temperature and pH 7.0. The pH was not extended beyond this value in order to avoid metal precipitation (Schiewer & Volesky 1995; Akar *et al.* 2009; Montazer-Rahmati *et al.* 2011), while at lower pH the $H^+$ ions are preferentially adsorbed (Torab-Mostaedi *et al.* 2013). Figure 4 illustrates the data of Cd(II) and Ni(II) ions adsorption by the magnetic nanopowder. At high metal ions, the graphs show a plateau typical of type L of the Langmuir model.

The linearized Langmuir and Freundlich equations for the metal ions removal from solutions are shown (Figure 5) and their calculated constants ($q_m$, $K_L$, $K_F$, and $n$) with correlation ($r^2$) values are tabulated (Table 2). By looking at the Ni(II) ions removal data, we can see that $r^2$ values are almost equal to unity, indicating that their adsorption fits Langmuir at 313 and 328 K while at 298 the isotherm fits better to the Freundlich model. Nevertheless, the Langmuir model fits better the adsorption equilibrium data Cd(II) ions.

**Table 1** | $N_2$ adsorption analysis data

| Property | Value |
|---|---|
| t-plot external surface area | 4.5294 $m^2/g$ |
| BET surface area | 4.5135 $m^2/g$ |
| Pore volume | 0.0201 $cm^3/g$ |
| Pore size (from distribution plot) | 36.0 A° |
| BJH adsorption size | 177.76 A° |
| BJH desorption size | 184.58 A° |

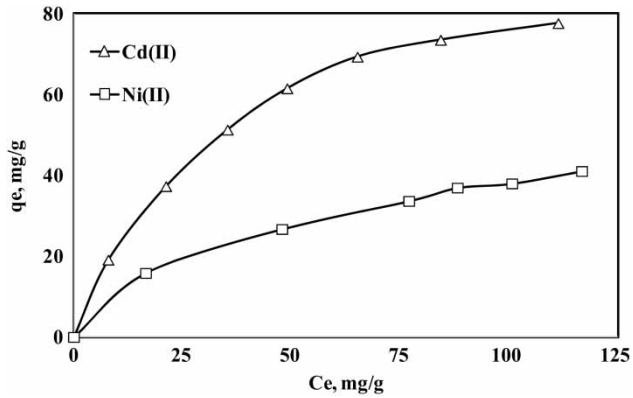


**Figure 4** | Adsorption equilibrium isotherms of Cd(II) and Ni(II) at 25 °C.

The obtained data also indicate that the adsorption of both metal ions is favorable at higher temperature. Moreover, the maximum adsorption capacity of the nanoparticles towards Cd(II) is about 128.21 $mg \cdot g^{-1}$, which was remarkably higher in comparison to the 82.65 $mg \cdot g^{-1}$ value for Ni(II) at highest temperature.

### Kinetic study

The kinetics data for Cd(II) and Ni(II) sorption as a function of time are shown in Figure 6 for the nanopowder at 298 K. It is evident that a sharp rise in the adsorption capacities $q_t$ takes place at the beginning and becomes steady after 100 minutes. Accordingly, this time was considered as the equilibrium time for both metal ions adsorption.

Figure 7(a) and 7(b) display the pseudo-first-order and the pseudo-second-order plots versus time sequentially. In Figure 7(a), ln $(q_e - q_t)$ versus $t$ graph is represented. The plot shows linearity with regression coefficient 0.9615 and 0.9388 for cadmium and nickel ions adsorption, respectively. While the $t/q_t$ against t-plot describing the pseudo-second-order law (Figure 7(b)) represents a better fitting for the data ($r^2 > 0.99$). On the other hand, the calculated $q_m$ values are in agreement with those obtained experimentally (Table 3). The obtained data clearly show the adsorption kinetics of both metal ions and suggests that kinetics in Cd(II) and Ni(II) adsorption follows the pseudo-second-order kinetic law. These findings agree well with previously reported data (Chen *et al.* 2008; Montazer-Rahmati *et al.* 2011).

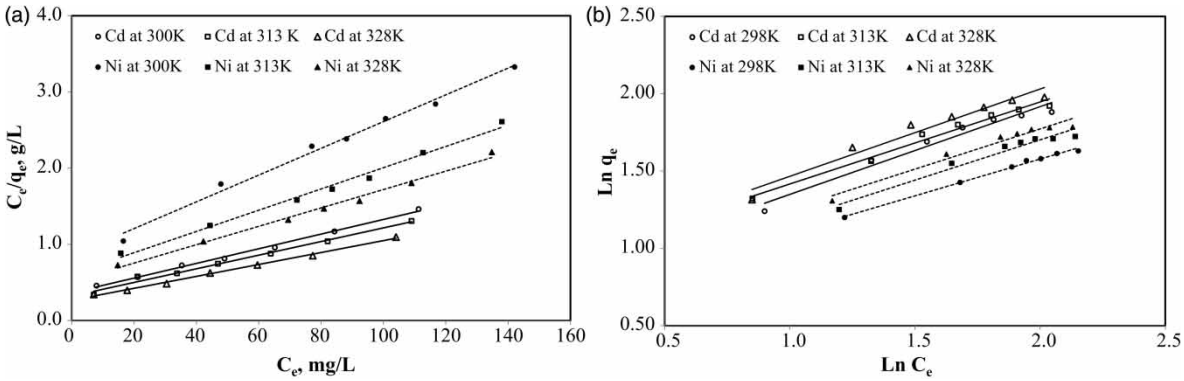


**Figure 5** | (a) Langmuir and (b) Freundlich adsorption isotherms of Cd(II) and Ni(II) at different temperatures.

**Table 2** | Langmuir and Freundlich isotherm parameters for the metal ions removal

| | | Langmuir constants | | | Freundlich constants | | |
|---|---|---|---|---|---|---|---|
| **Metal ion** | **T(K)** | $q_m$ (mg·g$^{-1}$) | $K_L$ (L·mg$^{-1}$) | $r^2$ | $n$ | $k_f$ | $r^2$ |
| Ni (II) | 298 | 57.14 | 0.0204 | 0.9906 | 2.099 | 4.21 | 0.9947 |
| | 313 | 71.94 | 0.0227 | 0.9926 | 1.9201 | 4.57 | 0.9592 |
| | 328 | 82.65 | 0.0236 | 0.9917 | 1.9231 | 5.39 | 0.9624 |
| Cd (II) | 298 | 104.17 | 0.0264 | 0.9960 | 1.837 | 6.80 | 0.9706 |
| | 313 | 111.12 | 0.0281 | 0.9885 | 1.886 | 7.69 | 0.9800 |
| | 328 | 128.21 | 0.0294 | 0.9961 | 1.7717 | 7.97 | 0.9559 |

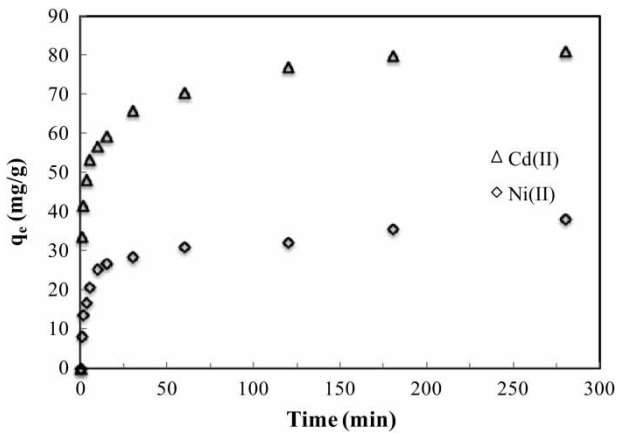


**Figure 6** | Adsorption of Cd(II) and Ni(II) on the (x)ZnO(1 – x)$Fe_2O_3$ nanopowder as a function of time.

## Thermodynamic study

The variation of metal ions adsorption with temperature was tested at 298, 313, and 328 K. The quantity of Cd(II) and Ni(II) eliminated by the ferrite magnetic particles increases with the rise in temperature, as presented by Figure 8 of the Langmuir model.

Considering the results obtained in the section 'Equilibrium study', only the Langmuir isotherm is tested to model the experimentally obtained data. Langmuir equation constants are listed in Table 4.

The enthalpy ($\Delta H^o$) value is calculated from ln($K_a$) versus $T^{-1}$ plot of Figure 9. The values of ($\Delta G^o$) and ($\Delta S^o$) are obtained mathematically from Equations (7) and (8). In Table 4, the thermodynamic function of adsorption is summarized. The adsorption can be described as endothermic according to $\Delta H^0$ positive value. The entropy values are positive for metal ions adsorption indicating enhanced randomness at the solid–solution interface.

As can be seen from the tabulated data $\Delta G^o < 0$ indicates a feasible, spontaneous physisorption process. In addition, this indicates favorable adsorption at higher temperature in correlation with the decreasing $\Delta G^o$ values as the solution is heated.

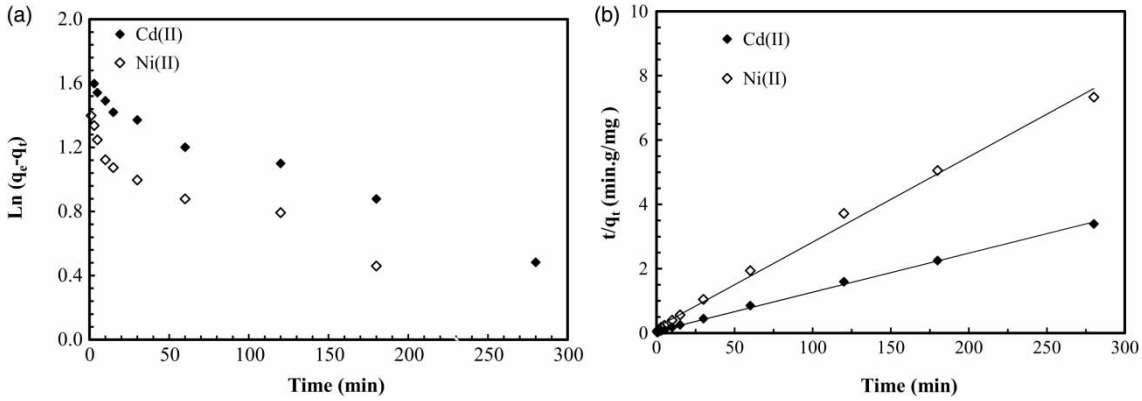


**Figure 7** | Kinetics of Cd(II) and Ni(II) adsorption onto the (x)ZnO(1 – x)$Fe_2O_3$: (a) pseudo-first-order plot and (b) pseudo-second-order plot.

**Table 3** | Rate constants for Cd(II) and Ni(II) ions adsorption on the adsorbent

| | | | | First-order | | | Second-order | | |
|---|---|---|---|---|---|---|---|---|---|
| **Metal ions** | $t_{1/2}$ (s) | $D \times 10^{15}$ ($cm^2 s^{-1}$) | $q^a_{m(exp)}$ ($mg \cdot g^{-1}$) | $k_1 \times 10^3$ ($min^{-1}$) | $q^b_{m(cal)}$ ($mg \cdot g^{-1}$) | $r^2$ | $k_2 \times 10^3$ ($g.(mg \cdot min)^{-1}$) | $q^b_{m(cal)}$ ($mg \cdot g^{-1}$) | $r^2$ |
| Cd (II) | 245.4 | 3.7 | 82.45 | 4.6 | 33.78 | 0.9615 | 3.01 | 81.3 | 0.9990 |
| Ni(II) | 398.4 | 2.3 | 38.03 | 5.7 | 19.14 | 0.9388 | 3.99 | 37.74 | 0.9952 |

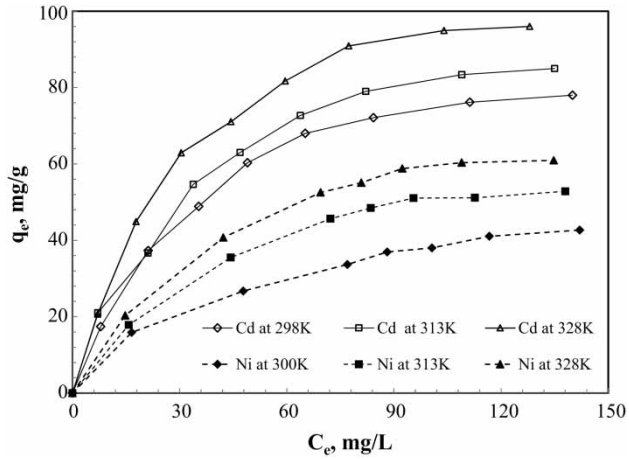


**Figure 8** | Langmuir isotherms for adsorption of Cd(II) and Ni(II) onto nanopowder material at different temperatures.

## Mechanism of adsorption

The adsorbed species may also be transported from solutions to a solid phase through intra-particle diffusion or transport process. Intra-particular diffusion is the limiting step for the sorption–desorption phenomenon. The Weber Morris mode is the formula used to describe the mechanism by which intra-particles can diffuse (Weber & Morris 1963; Mckay *et al.* 1980; Mckay 1983):

$$q_t = k_{dif}.t^{1/2} + C \quad (9)$$

where $C$ is a constant and $k_{dif}$ is the rate constant for intra-particle diffusion. The $k_{dif}$ values for the tested adsorbent are obtained as slopes of the graphs (Figure 10) and reported in Table 5. The uptake of cadmium and nickel ions at the surface of the magnetic particles may be governed by the intra-particle diffusion kinetics, since the $q_t$ values are linear correlation with $t_{1/2}$. The regression coefficient values are ≈1.0, indicating the applicability of this model. The intra-particle diffusion plots are shown in Figure 10, where the main parameters of this model are determined and gathered in Table 5. The values of $C$, obtained from the intercept of the graph, are the measure of the boundary layer effects or the extent of resistance to external mass diffusion. A greater value of $C$ indicates larger thickness of the boundary layer.

According to Li *et al.* (2012), in a multistep diffusion graph, the first sharp section represents a fast adsorption process instantaneously taking place at the outer surface. The

**Table 4** | Thermodynamic parameters for Ni(II) and Cd(II) adsorption

| Metal ions | Temperature (K) | *Ka* | $\Delta G^o$ (kJ·mol$^{-1}$) | $\Delta S^o$ (kJ·mol$^{-1}$·K$^{-1}$) | $\Delta H^o$ (kJ·mol$^{-1}$) | $r^2$ |
|---|---|---|---|---|---|---|
| | 298 | 1.168 | −0.385 | 0.0482 | 13.98 | 0.9788 |
| Ni(II) | 306 | 1.633 | −1.276 | 0.0488 | | |
| | 313 | 1.953 | −1.825 | 0.0482 | | |
| | 298 | 2.748 | −2.505 | 0.0371 | 8.55 | 0.9808 |
| Cd(II) | 306 | 3.122 | −2.963 | 0.0368 | | |
| | 313 | 3.772 | −3.621 | 0.0371 | | |

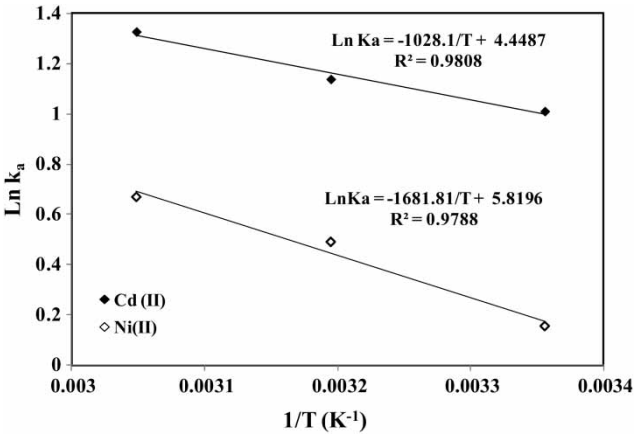


**Figure 9** | ln($K_a$) versus the reciprocal temperature of cadmium ion and nickel adsorption.

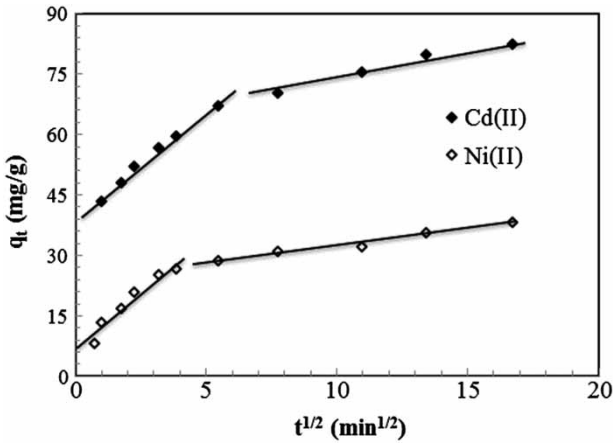


**Figure 10** | $q_t$ versus $t^{1/2}$ plot for the intraparticle diffusion.

second step is a slow adsorption stage or the diffusion rate-determining step is attributed to intra-particle diffusion. The lines of the graph (Figure 10) deviate from the origin, indicating considerable boundary layer control. The graph clearly shows two steps, implying that the diffusion of the metal ions is controlled not only by intra-particle diffusion but other kinetics processes may be involved (Arami *et al.* 2008).

Using Equation (10), the diffusivity that greatly depends on the adsorbent's surface is calculated (Yadava *et al.* 1987):

$$D = \frac{0.03 * r_0^2}{t_{1/2}} \tag{10}$$

where $D$ is the mass diffusivity and $r_0$ is the spherical-equivalent radius of the adsorbent particle (cm). Taking the particles' radius from the XRD calculations as equal to $5.5 \times 10^{-6}$ cm, the $D$ values were found to be $3.7 \times 10^{-9}$ and $2.3 \times 10^{-9}$ cm$^2$ s$^{-1}$ for $Cd^{+2}$ and $Ni^{+2}$ diffusion, respectively. The diffusivity values clearly indicate the preferential tendency of adsorbent to remove cadmium rather than nickel ions.

## COMPARISON OF $ZNFE_2O_4$ ADSORPTION CAPACITY WITH OTHER ADSORBENTS FOR CADMIUM AND NICKEL METAL IONS

The ability of the synthesized magnetic particles to eliminate the heavy metal ions under investigation was contrasted with other adsorbents reported in the literature, as listed in Table 6. The adsorbent employed in this study showed better adsorption performance than others, indicating that

**Table 5** | Intra-particle diffusion model parameters for Cd(II) and Ni(II) ions adsorption

| Metal ions | $k_{dif1}$, mg/g·min$^{1/2}$ | *c* | $r^2$ | $k_{dif\ 2}$, mg/g·min$^{1/2}$ | *c* | $r^2$ |
|---|---|---|---|---|---|---|
| Cd(II) | 5.199 | 39.33 | 0.989 | 1.38 | 60.22 | 0.9714 |
| Ni(II) | 5.621 | 6.585 | 0.9492 | 0.8434 | 23.952 | 0.9802 |

**Table 6** | A comparison of (x)ZnO(1 – x)$Fe_2O_3$ adsorption capacity with other adsorbents for cadmium and nickel metal ions

| Adsorbent | *Ni(II)* (mg·g$^{-1}$) | *Cd(II)* (mg·g$^{-1}$) | Temp. (K) | Reference |
|---|---|---|---|---|
| Silica-gel-biomass | 98.01 | – | 298 | Akar *et al.* (2009) |
| $CuFe_2O_4$ nano-particles | – | 17.54 | 298 | Tu *et al.* (2012) |
| $NH_2$-MCM-41 | 12.36 | 18.25 | 298 | Heidari *et al.* (2009) |
| Magnetic graphene oxide | – | 91.29 | 298 | Deng *et al.* (2013) |
| Milled goethite | – | 125 | 298 | Khezami *et al.* (2016) |
| Milled goethite | – | 167 | 328 | Khezami *et al.* (2016) |
| Ni (15% wt)-doped $\alpha$-$Fe_2O_3$ | – | 90.91 | 328 | OuldM'hamed *et al.* (2015) |
| Magnetic nanoparticles | 11.53 | – | 298 | Sharma & Srivastava (2010) |
| Lemon peel | 80.0 | – | 298 | Thirumavalavan *et al.* (2011) |
| Orange peel | 81.3 | – | 298 | Thirumavalavan *et al.* (2011) |
| $ZnFe_2O_4$ | 57.1 | 104.2 | 298 | Present work |
| $ZnFe_2O_4$ | 83 | 128 | 328 | Present work |

the tested nanopowder is a good candidate for cadmium and nickel ions removal from aqueous solutions.

## CONCLUSION

Magnetic nanoparticles (x)ZnO(1 – x)$Fe_2O_3$ were prepared by mechanical milling of commercial ingredient samples. Their ability to eliminate nickel and cadmium ions was investigated under different experimental conditions. The adsorption data at equilibrium were found to comply with the Langmuir isotherm for Cd(II) and with both the Langmuir and the Freundlich for Ni(II). At all temperatures, the magnetic nanoparticles removed larger amounts of cadmium (128 mg·L$^{-1}$) than nickel ions (83 mg·L$^{-1}$) at 328 K. Furthermore, the kinetics follows the second-order rate law. The thermodynamic data revealed an endothermic, spontaneous, physisorption process. The suggested adsorption mechanism indicated that the process controlled intra-particle diffusion along with other kinetic models.

## ACKNOWLEDGEMENTS

The authors would like to thank the National Plan for Sciences, Technology and Innovation (MAARIFAH), King Abdulaziz City for Sciences & Technology, Kingdom of Saudi Arabia.

## REFERENCES

Akar, T., Kaynak, Z., Ulusoy, S., Yuvaci, D., Ozsari, G. & Akar, S. T. 2009 Enhanced biosorption of nickel(II) ions by silica-gel-immobilized waste biomass: biosorption characteristics in batch and dynamic flow mode. *Journal of Hazardous Materials* **163** (2), 1134–1141.

Arami, M., Limaee, N. Y. & Mahmoodi, N. M. 2008 Evaluation of the adsorption kinetics and equilibrium for the potential removal of acid dyes using a biosorbent. *Chemical Engineering Journal* **139** (1), 2–10.

Arce, V. B., Gargarello, R. M., Ortega, F., Romañano, V., Mizrahi, M., Ramallo-López, J. M., Cobos, C. J., Airoldi, C., Bernardelli, C. & Donati, E. R. 2015 EXAFS and DFT study of the cadmium and lead adsorption on modified silica nanoparticles. *Spectrochimica Acta Part A: Molecular and Biomolecular Spectroscopy* **151**, 156–163.

Babel, S. & Kurniawan, T. A. 2004 Cr(VI) removal from synthetic wastewater using coconut shell charcoal and commercial activated carbon modified with oxidizing agents and/or chitosan. *Chemosphere* **54** (7), 951–967.

Bhowmik, K., Debnath, A., Nath, R., Das, S., Chattopadhyay, K. & Saha, B. 2016 Synthesis and characterization of mixed phase manganese ferrite and hausmannite magnetic nanoparticle as potential adsorbent for methyl orange from aqueous media: artificial neural network modeling. *Journal of Molecular Liquids* **219**, 1010–1022.

Boparai, H. K., Joseph, M. & O'Carroll, D. M. 2011 Kinetics and thermodynamics of cadmium ion removal by adsorption onto

nano zerovalent iron particles. *Journal of Hazardous Materials* **186** (1), 458–465.

Chen, Z., Ma, W. & Han, M. 2008 Biosorption of nickel and copper onto treated alga (Undaria pinnatifida): application of isotherm and kinetic models. *Journal of Hazardous Materials* **155** (1), 327–333.

Chen, D., Li, L. & Wang, J.-H. 2013 One-step synthesis of zinc ferrite nanoparticles by ultrasonic wave-assisted ball milling technology. *Ceramics International* **39** (4), 4669–4672.

Debnath, A., Majumder, M., Pal, M., Das, N. S., Chattopadhyay, K. K. & Saha, B. 2016 Enhanced adsorption of hexavalent chromium onto magnetic calcium ferrite nanoparticles: kinetic, isotherm, and neural network modeling. *Journal of Dispersion Science and Technology* **37** (12), 1806–1818.

Deng, J.-H., Zhang, X.-R., Zeng, G.-M., Gong, J.-L., Niu, Q.-Y. & Liang, J. 2013 Simultaneous removal of Cd(II) and ionic dyes from aqueous solution using magnetic graphene oxide nanocomposite as an adsorbent. *Chemical Engineering Journal* **226**, 189–200.

Ding, Z., Wang, W., Zhang, Y., Li, F. & Liu, J. P. 2015 Synthesis, characterization and adsorption capability for Congo red of $CoFe_2O_4$ ferrite nanoparticles. *Journal of Alloys and Compounds* **640**, 362–370.

Fu, F. & Wang, Q. 2011 Removal of heavy metal ions from wastewaters: a review. *Journal of Environmental Management* **92** (3), 407–418.

Guo, R., Fang, L., Dong, W., Zheng, F. & Shen, M. 2011 Magnetically separable bifeo$_3$ nanoparticles with a $\gamma$-$Fe_2O_3$ parasitic phase: controlled fabrication and enhanced visible-light photocatalytic activity. *Journal of Materials Chemistry* **21** (46), 18645–18652.

Gupta, V., Sharma, S., Yadav, I. & Mohan, D. 1998 Utilization of bagasse fly ash generated in the sugar industry for the removal and recovery of phenol and p-nitrophenol from wastewater. *Journal of Chemical Technology and Biotechnology* **71** (2), 180–186.

Heidari, A., Younesi, H. & Mehraban, Z. 2009 Removal of Ni(II), Cd(II), and Pb(II) from a ternary aqueous solution by amino functionalized mesoporous and nano mesoporous silica. *Chemical Engineering Journal* **153** (1), 70–79.

Ho, Y.-S. & McKay, G. 1998 Sorption of dye from aqueous solution by peat. *Chemical Engineering Journal* **70** (2), 115–124.

Kale, A., Gubbala, S. & Misra, R. 2004 Magnetic behavior of nanocrystalline nickel ferrite synthesized by the reverse micelle technique. *Journal of Magnetism and Magnetic Materials* **277** (3), 350–358.

Khezami, L., Ould M'hamed, M., Lemine, O., Bououdina, M. & Bessadok-Jemai, A. 2016 Milled goethite nanocrystalline for selective and fast uptake of cadmium ions from aqueous solution. *Desalination and Water Treatment* **57** (14), 6531–6539.

Kodama, R. H., Berkowitz, A. E., McNiff Jr, E. & Foner, S. 1996 Surface spin disorder in $NiFe_2O_4$ nanoparticles. *Physical Review Letters* **77** (2), 394–397.

Li, Q., Zhai, J., Zhang, W., Wang, M. & Zhou, J. 2007 Kinetic studies of adsorption of Pb(II), Cr(III) and Cu(II) from aqueous solution by sawdust and modified peanut husk. *Journal of Hazardous Materials* **141** (1), 163–167.

Li, Z., Katsumi, T., Imaizumi, S., Tang, X. & Inui, T. 2010 Cd (II) adsorption on various adsorbents obtained from charred biomaterials. *Journal of Hazardous Materials* **183** (1), 410–420.

Li, Y., Du, Q., Liu, T., Sun, J., Jiao, Y., Xia, Y., Xia, L., Wang, Z., Zhang, W. & Wang, K. 2012 Equilibrium, kinetic and thermodynamic studies on the adsorption of phenol onto graphene. *Materials Research Bulletin* **47** (8), 1898–1904.

Lippens, B. C. & De Boer, J. 1965 Studies on pore systems in catalysts: v. The t method. *Journal of Catalysis* **4** (3), 319–323.

Mckay, G. 1983 The adsorption of dyestuffs from aqueous solutions using activated carbon. III. Intraparticle diffusion processes. *Journal of Chemical Technology and Biotechnology. Chemical Technology* **33** (4), 196–204.

Mckay, G., Otterburn, M. & Sweeney, A. 1980 The removal of colour from effluent using various adsorbents – III. Silica: rate processes. *Water Research* **14** (1), 15–20.

Meena, A. K., Mishra, G., Rai, P., Rajagopal, C. & Nagar, P. 2005 Removal of heavy metal ions from aqueous solutions using carbon aerogel as an adsorbent. *Journal of Hazardous Materials* **122** (1), 161–170.

Montazer-Rahmati, M. M., Rabbani, P., Abdolali, A. & Keshtkar, A. R. 2011 Kinetics and equilibrium studies on biosorption of cadmium, lead, and nickel ions from aqueous solutions by intact and chemically modified brown algae. *Journal of Hazardous Materials* **185** (1), 401–407.

Mozaffari, M., Arani, M. E. & Amighian, J. 2010 The effect of cation distribution on magnetization of $ZnFe_2O_4$ nanoparticles. *Journal of Magnetism and Magnetic Materials* **322** (21), 3240–3244.

Nassar, M. Y. & Khatab, M. 2016 Cobalt ferrite nanoparticles via a template-free hydrothermal route as an efficient nano-adsorbent for potential textile dye removal. *RSC Advances* **6** (83), 79688–79705.

Nordberg, G. F., Fowler, B. A. & Nordberg, M. 2014 *Handbook on the Toxicology of Metals.* Academic Press, London.

OuldM'hamed, M., Khezami, L., Alshammari, A. G., Ould-Mame, S., Ghiloufi, I. & Lemine, O. 2015 Removal of cadmium(II) ions from aqueous solution using Ni (15 wt.%)-doped $\alpha$-$Fe_2O_3$ nanocrystals: equilibrium, thermodynamic, and kinetic studies. *Water Science and Technology* **72** (4), 608–615.

Ramana, D. V., Yu, J. S. & Seshaiah, K. 2013 Silver nanoparticles deposited multiwalled carbon nanotubes for removal of Cu(II) and Cd(II) from water: surface, kinetic, equilibrium, and thermal adsorption properties. *Chemical Engineering Journal* **223**, 806–815.

Reddy, D. H. K. & Yun, Y.-S. 2016 Spinel ferrite magnetic adsorbents: alternative future materials for water purification? *Coordination Chemistry Reviews* **315**, 90–111.

Rouquerol, J., Rouquerol, F., Llewellyn, P., Maurin, G. & Sing, K. S. 2013 *Adsorption by Powders and Porous Solids:*

*Principles, Methodology and Applications*. Academic Press, London.

Roy, A. & Bhattacharya, J. 2013 A binary and ternary adsorption study of wastewater Cd(II), Ni(II) and Co(II) by $\gamma$-$Fe_2O_3$ nanotubes. *Separation and Purification Technology* **115**, 172–179.

Roy, M., Haldar, B. & Verma, H. 2005 Characteristic length scales of nanosize zinc ferrite. *Nanotechnology* **17** (1), 232–237.

Sakthivel, S., Geissen, S.-U., Bahnemann, D., Murugesan, V. & Vogelpohl, A. 2002 Enhancement of photocatalytic activity by semiconductor heterojunctions: $\alpha$-$Fe_2O_3$, $WO_3$ and CdS deposited on ZnO. *Journal of Photochemistry and Photobiology A: Chemistry* **148** (1), 283–293.

Schiewer, S. & Volesky, B. 1995 Modeling of the proton-metal ion exchange in biosorption. *Environmental Science & Technology* **29** (12), 3049–3058.

Sharma, Y. & Srivastava, V. 2010 Comparative studies of removal of Cr(VI) and Ni(II) from aqueous solutions by magnetic nanoparticles. *Journal of Chemical & Engineering Data* **56** (4), 819–825.

Singh, D., Rupainwar, D., Prasad, G. & Jayaprakas, K. 1998 Studies on the Cd(II) removal from water by adsorption. *Journal of Hazardous Materials* **60** (1), 29–40.

Tang, S. C. & Lo, I. M. 2013 Magnetic nanoparticles: essential factors for sustainable environmental applications. *Water Research* **47** (8), 2613–2632.

Thirumavalavan, M., Lai, Y.-L. & Lee, J.-F. 2011 Fourier transform infrared spectroscopic analysis of fruit peels before and after the adsorption of heavy metal ions from aqueous solution. *Journal of Chemical & Engineering Data* **56** (5), 2249–2255.

Thirupathi, G. & Singh, R. 2015 Study of magnetoviscosity of ferromagnetic MnZn-ferrite ferrofluid. *IEEE Transactions on Magnetics* **51** (11), 1–4.

Torab-Mostaedi, M., Asadollahzadeh, M., Hemmati, A. & Khosravi, A. 2013 Equilibrium, kinetic, and thermodynamic studies for biosorption of cadmium and nickel on grapefruit peel. *Journal of the Taiwan Institute of Chemical Engineers* **44** (2), 295–302.

Tu, Y.-J., You, C.-F. & Chang, C.-K. 2012 Kinetics and thermodynamics of adsorption for Cd on green manufactured nano-particles. *Journal of Hazardous Materials* **235**, 116–122.

Weber, W. J. & Morris, J. C. 1963 Kinetics of adsorption on carbon from solution. *Journal of the Sanitary Engineering Division* **89** (2), 31–60.

Weng, C.-H. & Huang, C. 2004 Adsorption characteristics of Zn(II) from dilute aqueous solution by fly ash. *Colloids and Surfaces A: Physicochemical and Engineering Aspects* **247** (1), 137–143.

Xu, P., Zeng, G. M., Huang, D. L., Feng, C. L., Hu, S., Zhao, M. H., Lai, C., Wei, Z., Huang, C. & Xie, G. X. 2012 Use of iron oxide nanomaterials in wastewater treatment: a review. *Science of the Total Environment* **424**, 1–10.

Yadava, K., Tyagi, B., Panday, K. & Singh, V. 1987 Fly ash for the treatment of Cd(II) rich effluents. *Environmental Technology* **8** (1–12), 225–234.

Zhang, J., Xiao, X. & Nan, J. 2010 Hydrothermal-hydrolysis synthesis and photocatalytic properties of nano-$TiO_2$ with an adjustable crystalline structure. *Journal of Hazardous Materials* **176** (1), 617–622.

First received 19 February 2017; accepted in revised form 23 May 2017. Available online 30 June 2017